Mechanism for Activation of Molecular Oxygen by cis- and trans-(Pyridine)(2)Pd(OAc)H: Pd-0 versus Direct Insertion

2 AUTHORS:

Jason Keith
Colgate University
28 PUBLICATIONS **487** CITATIONS

SEE PROFILE

William A. Goddard
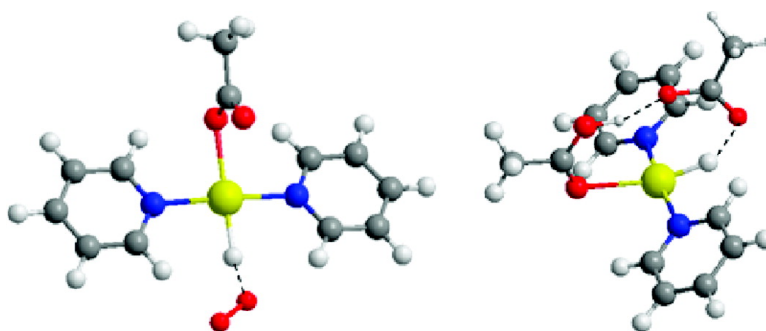California Institute of Technology
1,332 PUBLICATIONS **68,116** CITATIONS

SEE PROFILE

Mechanism for Activation of Molecular Oxygen by *cis*- and *trans*-(Pyridine)Pd(OAc)H: Pd versus Direct Insertion

Jason M. Keith, and William A. Goddard III

More About This Article

Additional resources and features associated with this article are available within the HTML version:

- Supporting Information
- Access to high resolution figures
- Links to articles and content related to this article
- Copyright permission to reproduce figures and/or text from this article

View the Full Text HTML

Mechanism for Activation of Molecular Oxygen by *cis*- and *trans*-(Pyridine)₂Pd(OAc)H: Pd⁰ versus Direct Insertion

Jason M. Keith and William A. Goddard III*

Materials Process and Simulation Center, MC (139-74), California Institute of Technology, Pasadena, California 91125

Received May 29, 2008; E-mail: wag@wag.caltech.edu

Abstract: We use quantum mechanics to elucidate the mechanism for the reaction of molecular oxygen with palladium–hydride complexes, (pyridine)₂–Pd^{II}(H)OAc, in toluene, focusing specifically on the direct insertion pathway of dioxygen into the Pd–H bond and pathways proceeding through a Pd⁰ intermediate for both cis and trans starting configurations as well as with the assistance of an extra HOAc molecule We report the potential energy surfaces and structures for each of these pathways. This is the first examination of these two mechanisms for both cis and trans isomers of a system employing two monodentate ligands. It is the first case of acid-assisted reductive elimination from a square planar Pd–H. The calculated mechanisms indicate that cis/trans isomerization is feasible and demonstrates that the Pd⁰ pathway is favored for both cis ($\Delta\Delta H^{\ddagger} = 2.2$ kcal/mol, $\Delta\Delta G^{\ddagger} = 9.3$ kcal/mol) and trans cases (HOAc-assisted; $\Delta\Delta H^{\ddagger} = -2.6$ kcal/mol, $\Delta\Delta G^{\ddagger} = 5.8$ kcal/mol) demonstrating that the presence of two monodentate ligands changes the mechanism from that of the bidentate case.

1. Introduction

Palladium oxidation catalysis employing molecular oxygen as the stoichiometric oxidant has become ubiquitous.[1] Oxygen is inexpensive, abundant, noncorrosive, and environmentally benign making it the ideal oxidant for green chemistry. Thus, it is highly desirable to enable the use of molecular oxygen. Indeed, Pd/O₂ systems have been developed for selective oxidation of alcohols,[2] intermolecular oxidative amination of alkenes,[3] oxidative C–C bond cleavage in tertiary alcohols,[4] intermolecular heterocyclization of alkenes,[5] and the synthesis of hydrogen peroxide.[6] Nevertheless, only a fraction of the important reactions involving Pd systems utilize dioxygen, leaving numerous reactions where the use of oxygen as the stoichiometric oxidant would be valuable.[1a,b]

These palladium-catalyzed oxidations are believed to proceed through an "oxidase" pathway, in which oxidation of the substrate by the palladium species occurs first, followed by reoxidation of palladium by O₂ (Scheme 1). Despite the general acceptance of the mechanism, the specific details of the reoxidation are actively debated. In order to provide the mechanistic understanding to aid rational design of new catalysts, we examine here the two main pathways expected to account for the majority of the systems involved:[7−9]

1 direct insertion of O₂ into a Pd^{II}–hydride brought about by the abstraction of the hydrogen atom by O₂ followed by

(1) (a) Nishimura, T.; Uemura, S. *Synlett* **2004**, *2*, 201. (b) Stahl, S. S. *Angew. Chem., Int. Ed.* **2004**, *43*, 3400. (c) Gligorich, K. M.; Sigman, M. S. *Angew. Chem., Int. Ed.* **2006**, *45*, 6612. (d) Stoltz, B. M. *Chem. Lett.* **2004**, 362. (e) Sigman, M. S.; Schultz, M. J. *Org. Biomol. Chem.* **2004**, *2*, 2551. (f) Stahl, S. *Science* **2005**, *309*, 1824. (g) Sigman, M. S.; Jensen, D. R. *Acc. Chem. Res.* **2006**, *39*, 221. (h) Sheldon, R. A.; Arends, I. W. C. E.; ten Brink, G.-J.; Dijksman, A. *Acc. Chem. Res.* **2002**, *35*, 774. (i) Toyota, M.; Ihara, M. *Synlett* **2002**, 1211.

(2) (a) Sigman, M. S.; Jensen, D. R. *Acc. Chem. Res.* **2006**, *39*, 221. (b) Bagdanoff, J. T.; Stoltz, B. M. *Angew. Chem., Int. Ed.* **2004**, *43*, 353. (c) Jensen, D. R.; Schultz, M. J.; Mueller, J. A.; Sigman, M. S. *Angew. Chem., Int. Ed.* **2003**, *42*, 3810. (d) Schultz, M. J.; Park, C. C.; Sigman, M. S. *Chem. Commun.* **2002**, 3034. (e) Bagdanoff, J. T.; Ferreira, E. M.; Stoltz, B. M. *Org. Lett.* **2003**, *5*, 835. (f) Jensen, D. R.; Sigman, M. S. *Org. Lett.* **2003**, *5*, 63. (g) Ferreira, E. M.; Stoltz, B. M. *J. Am. Chem. Soc.* **2001**, *123*, 7725. (h) Steinhoff, B. A.; Stahl, S. S. *Org. Lett.* **2002**, *4*, 4179.

(3) (a) Rogers, M. M.; Wendlandt, J. E.; Guzei, I. A.; Stahl, S. S. *Org. Lett.* **2006**, *8*, 2257. (b) Lee, J. M.; Ahn, D. S.; Jung, D. Y.; Lee, J.; Do, Y.; Kim, S. K.; Chang, S. K. *J. Am. Chem. Soc.* **2006**, *128*, 12954. (c) Streuff, J.; Hovelmann, C. H.; Nieger, M.; Muniz, K. *J. Am. Chem. Soc.* **2005**, *127*, 14586. (d) Brice, J. L.; Harang, J. E.; Timokhin, V. I.; Anastasi, N. R.; Stahl, S. S. *J. Am. Chem. Soc.* **2005**, *127*, 2868. (e) Timokhin, V. I.; Anastasi, N. R.; Stahl, S. S. *J. Am. Chem. Soc.* **2003**, *125*, 12996.

(4) (a) Nishimura, T.; Araki, H.; Maeda, Y.; Uemura, S. *Org. Lett.* **2003**, *5*, 2997. (b) Matsumura, S.; Maeda, Y.; Nishimura, T.; Uemura, S. *J. Am. Chem. Soc.* **2003**, *125*, 8862. (c) Nishimura, T.; Matsumura, S.; Maeda, Y.; Uemura, S. *Tetrahedron Lett.* **2002**, *43*, 3037. (d) Nishimura, T.; Ohe, K.; Uemura, S. *J. Am. Chem. Soc.* **1999**, *121*, 2645.

(5) (a) Piera, J.; Narhi, K.; Backvall, J. E. *Angew. Chem., Int. Ed.* **2006**, *45*, 6914. (b) Trend, R. M.; Ramtohul, Y. K.; Ferreira, E. M.; Stoltz, B. M. *Angew. Chem., Int. Ed.* **2003**, *42*, 2892.

(6) Bianchi, D.; Bortolo, R.; D'Aloisio, R.; Ricci, M. *Angew. Chem., Int. Ed.* **1999**, *38*, 706.

(7) (a) Keith, J. M.; Nielsen, R. J.; Oxgaard, J.; Goddard, W. A., III. *J. Am. Chem. Soc.* **2005**, *127*, 13172. (b) Keith, J. M.; Muller, R. P.; Kemp, R. A.; Goldberg, K. I.; Goddard, W. A., III. *Inorg. Chem.* **2006**, *45*, 9631. (c) Keith, J. M.; Goddard, W. A., III.; Oxgaard, J. *J. Am. Chem. Soc.* **2007**, *129*, 10361.

(8) (a) Denny, M. C.; Smythe, N. A.; Cetto, K. L.; Kemp, R. A.; Goldberg, K. I. *J. Am. Chem. Soc.* **2006**, *128*, 2508. (b) A second paper appearing shortly after that also reports insertion of molecular oxygen into a Pd^{II}–H bond: Konnick, M. M.; Gandhi, B. A.; Guzei, I. A.; Stahl, S. S. *Angew. Chem., Int. Ed.* **2006**, *45*, 2904.

(9) Two additional pathways proposed for this process are (1) the oxidative addition of O₂ to form an octahedral Pd^{IV} complex; (2) the substitution of O₂ for the X-ligand forming a cationic LPd^{III}H–superoxide. These pathways have been eliminated due to unreasonably high-energy intermediates and will not be examined here. For a thorough examination of all four of these pathways, see: Popp, B. V.; Stahl, S. S. *J. Am. Chem. Soc.* **2007**, *129*, 4410.
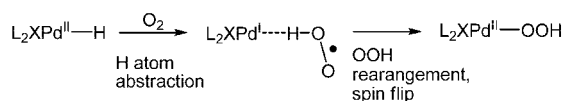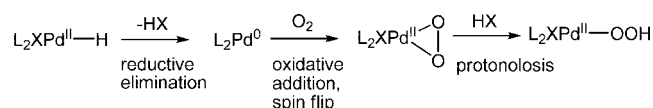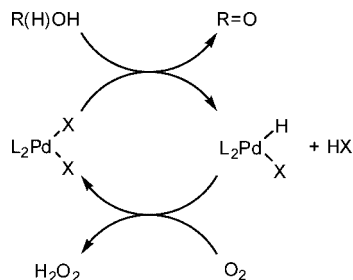
Direct Insertion

Pd⁰ Pathway

Figure 1. The two feasible mechanisms shown previously to be at work for the aerobic oxidation of L_2PdHX.

Scheme 1

rearrangement of the HOO• fragment and spin conversion (Figure 1, "Direct Insertion");

2 formation of Pd⁰ through the reductive elimination of HX followed by reaction with O_2 (Figure 1, "Pd⁰ Pathway").

Multiple experimental studies have been reported on the direct reaction of Pd⁰ with O_2, demonstrating both the formation of a stable η^2-peroxo Pd^{II} complex and the eventual products hydrogen peroxide and Pd$^{II}X_2$, after treatment with HX.[10] This demonstrates the feasibility but not conclusive proof of the Pd⁰ pathway under select conditions. In addition to the experimental work, Landis and co-workers used density functional theory (DFT) to examine the feasibility of a spin crossover for several Pd⁰ systems by examining the minimum energy crossing point (MECP) between the two surfaces and showed that a triplet Pd^{I}–superoxide complex is formed followed by conversion to a singlet Pd^{II}–peroxo complex that is significantly downhill, making the barrier for the spin crossing practically negligible.[10d,e]

The direct insertion mechanism was first demonstrated through DFT studies on a ((−)sparteine)PdHCl system we reported in 2005.[7a] The insertion mechanism was found to proceed through the abstraction of a hydrogen atom by dioxygen to form a Pd^{I} radical T-complex with HOO• that subsequently forms the triplet palladium hydroperoxo species. This biradical triplet crosses over to form the singlet hydroperoxo species, and the reaction then proceeds on the singlet surface through the addition of a proton to form H_2O_2 and the corresponding PdCl₂. We concluded that the reformation of the two radical species and the existence of the cis hydrogen-bond acceptor were intimately correlated and that removal of the cis hydrogen-bond acceptor substantially increases the reaction barrier as the radical pair must first undergo a spin conversion before directly forming

the singlet hydroperoxo species en route to completing the catalytic cycle.

Following our 2005 prediction of this new direct mechanism, Denny et al. published experimental results in 2006 involving a non-Pd⁰ insertion of O_2 into a Pd–H bond that demonstrated first-order kinetics with respect to oxygen, which is consistent with our direct insertion mechanism.[8] Later in 2006 we verified computationally that this new system of Denny et al. operates through the same direct insertion mechanism that we had previously demonstrated for the ((−)sparteine)PdHCl system.[7b] However, the ligand framework employed in the Denny system (a planar tridentate ligand with a central N-heterocyclic carbene and two phosphines) prevents the formation of Pd⁰ so that it does not provide information about the competition between the Pd⁰ and direct insertion pathways.

In order to examine the competition between these two mechanisms we examined the Pd⁰ pathway for the ((−)sparteine)-PdHCl system showing that the direct insertion is favored (by $\Delta\Delta H^{\ddagger} = 6.2$ kcal/mol, $\Delta\Delta G^{\ddagger} = 7.5$ kcal/mol).[7c] In this 2007 paper we postulated that this was most likely due to the bidentate character of the ligand that prevents the formation of a linear Pd⁰ species and the requirement of an exogenous base. This work also demonstrated that similar results are obtained using the spin conversion approach of Landis et al., in which feasible MECPs between the singlet and triplet palladium hydroperoxo and between several bound and unbound O_2 and OOH fragments were calculated.[10d] In further work with ((−)sparteine)PdHX we showed that this preference reverses with the substitution of OAc ion, due to its ability to chelate to the metal after the reductive elimination, removing the need for the exogenous base.[11]

Simultaneous with our results completing the ((−)sparteine)-PdClH study, Popp and Stahl published in 2007 a thorough examination of (IMes)₂PdHOAc (Figure 2).[9] Analogous to the combination of our 2005 and 2007 manuscripts[7a,c] Popp and Stahl examined both the direct insertion (which they referred to as "HX reductive elimination pathway") and Pd⁰ (which they referred to as "hydrogen-atom abstraction pathway") mechanisms for their system computationally. They demonstrated that the direct insertion mechanism is lower in energy than the Pd⁰ pathway ($\Delta\Delta H^{\ddagger} = 12.3$ kcal/mol, $\Delta\Delta G^{\ddagger} = 4.8$ kcal/mol) although they consider these barriers to be "very similar in energy" based on the assumed margin of error for their calculations. They concluded that the "[Pd⁰ pathway] is the most likely mechanism for catalyst oxidation under typical reaction conditions" in contradiction to their calculated results. They rationalize this discrepancy by alluding to the "tentative" results for the addition of exogenous carboxylic acid, which they found to lower the barrier for the Pd⁰ pathway by ∼1 kcal/mol on the ΔE surface, a result that would likely be counteracted if they had include entropy. Simplified drawings of their three main transition state structures are shown in Figure 2.

To rationalize these confounding results, we suggest that the conclusions and chemical intuition of Popp and Stahl are sound but that some issues in their computational picture are the culprit. First consider the angle θ in the transition states **a** and **b** of Figure 2. In **a** $\theta = \sim 87°$, whereas the reactant has $\theta = \sim 180°$, most likely contributing considerably to the barrier. They found that inclusion of an additional HOAc molecule increases θ only from ∼87 to ∼89. This seems strange as the additional acid

(10) (a) Konnick, M. M.; Guzei, I. A.; Stahl, S. S. *J. Am. Chem. Soc.* **2004**, *126*, 10212. (b) Stahl, S. S.; Thorman, J. L.; Nelson, R. C.; Kozee, M. A. *J. Am. Chem. Soc.* **2001**, *123*, 7188. (c) Clegg, W.; Eastham, G. R.; Elsegood, M. R. J.; Heaton, B. T.; Iggo, J. A.; Tooze, R. P.; Whyman, R.; Zacchini, S. *J. Chem. Soc., Dalton. Trans.* **2002**, 3300. (d) Landis, C. R.; Morales, C. M.; Stahl, S. S. *J. Am. Chem. Soc.* **2004**, *126*, 16302. (e) Popp, B. V.; Wendlandt, J. E.; Landis, C. R.; Stahl, S. S. *Angew. Chem., Int. Ed.* **2007**, *46*, 601.

(11) Keith, J. M.; Goddard, W. A., III. *Organometallics*, submitted for publication.
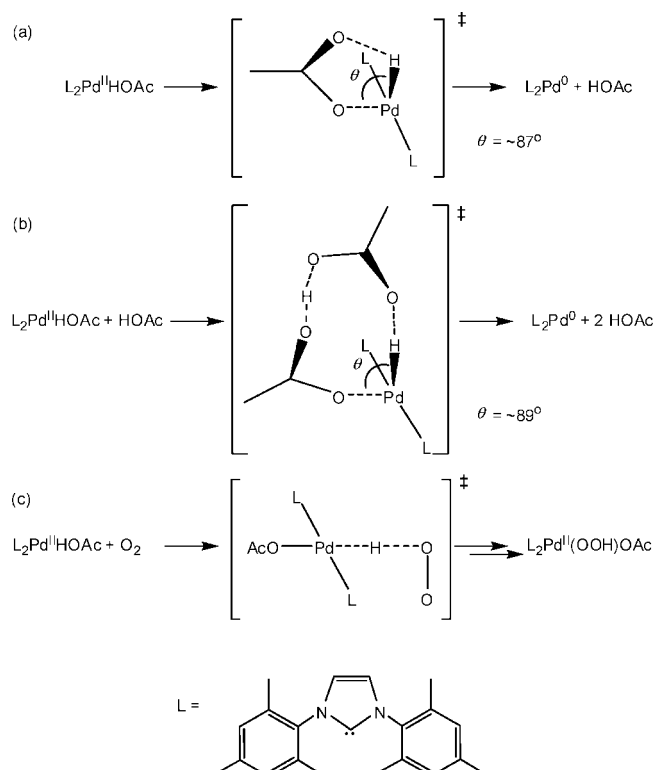
Figure 2. Transition state structures presented in study of *trans*-(IMes)$_2$PdHOAc + O$_2$ by Popp and Stahl (ref 9).

molecule should allow the transition state to relax further toward 180°. This might have occurred if the additional molecule was simply added to the previously optimized seesaw transition state and then optimized further rather than searching for the acid-assisted pathway that corresponds to the square planar structure.

Another possible source for the missing low-energy direct insertion mechanism in the Popp and Stahl study could possibly be the failure to examine any transition states arising from cis structures. Although Konnick et al. synthesized the trans species experimentally,[8b] we believe that both the cis and the trans species could be active in the catalytic systems. Evidence for this can be seen in the necessity of a cis ligand system for the β-hydride elimination mechanism for the reduction of alcohols by Pd^{II} complexes, resulting in the formation of *cis*-L$_2$Pd^{II}H-alkoxide and subsequently what is thought to be *cis*-L$_2$Pd^{II}HX.[12] The possible interconversion between the cis and trans species must also be examined at this point in the reaction mechanism. Although these suggestions play an important role in the calculations of our pyridine system discussed here, it is not known if they will affect the much bulkier N-heterocyclic carbene system discussed above.

Herein we present a detailed mechanistic examination of the reaction of O$_2$ with (pyr)$_2$PdHOAc, focusing on direct insertion and Pd^0 mechanisms for both the cis and trans species as well as the interconversion between the two and the acid-assisted *trans*-Pd^0 pathway that maintains a near square planar structure in the transition state (θ = 159.3). These new results provide a complete picture of both possible pathways for this system thus defining the preferred path and suggest ways to obtain consistent results for related systems.

2. Computational Methodology

All calculations were performed using the B3LYP hybrid DFT functional, which includes a fraction of exact Hartree−Fock exchange in addition to the Becke generalized gradient approximation in the exchange potential combined with the correlation functional of Lee, Yang, and Parr (LYP).[13−15] B3LYP is known to produce good descriptions of reaction profiles for transition metal containing compounds.[16,17]

Pd was described with the small core LACVP** effective core potential and basis set (18 explicit electrons).[18] For all other elements the core electrons were included explicitly, using the Pople 6-31G** basis set,[19] but with 3s combination of the six d-like functions reduced to five.

All geometries were optimized and the analytic Hessian evaluated to determine the number of imaginary frequencies through vibrational frequency calculations. In all cases the local minima had no imaginary frequencies, whereas the transition state structures led to exactly one imaginary frequency

Implicit solvent effects for toluene were calculated with the Poisson−Boltzmann (PBF) continuum approximation,[20] as implemented in the Jaguar 7.0 program package,[13] which uses standard vdW radii to construct the solvent-accessible surface of the molecular complex. The solvation energies were calculated at geometries optimized for the gas phase using the dielectric constant ε = 2.38 and solvent radius = 2.76 Å.

The vibrational frequencies from the analytic Hessian were used to calculate the zero-point energy corrections at 0 K, which was added to the solvation correction and the QM energy (Δ[E]) to obtain the enthalpy at 0 K, ΔH[0 K]. Similarly, the vibrational frequencies were used to calculate the entropy and enthalpy corrections to 298.15 K, to obtain (ΔH − TΔS) = ΔG [298.15 K].

On the basis of previous results we expect that relative energies on the ΔH[0 K] surface are accurate to ∼3 kcal/mol for stable intermediates and to ∼5 kcal/mol for transition structures. The relative energies on the ΔG [298 K] surface may be less accurate, due to the use of the PBF model.[21] This methodology was found to provide a useful level of theory in our previous study of ((−)sparteine)PdHCl.[7a]

We use the standard Kohn−Sham formalism to obtain self-consistent DFT orbitals for a wave function formulated in terms of a Slater determinant. This process is best suited for states that are well described as closed-shell (an up and down spin in each occupied orbital). However, it is particularly poor for describing the ground state of O$_2$, which has $^3\Sigma_g^-$ symmetry. Here one allows two more orbitals (one is π$_{gx}$ and the other π$_{gy}$) to have an up spin

(12) Nielsen, R. J.; Keith, J. M.; Stoltz, B. M.; Goddard, W. A., III. *J. Am. Chem. Soc.* **2004**, *126*, 7967.

(13) (a) Jaguar 7.0; Schrodinger, Inc.: Portland, OR, 2005. (b) See, for example: Greeley, B. H.; Russo, T. V.; Mainz, D. T.; Friesner, R. A.; Langlois, J.-M.; Goddard, W. A.; Donnelly, R. E.; Ringnalda, M. N. *J. Chem. Phys.* **1994**, *101*, 4028.

(14) Becke, A. D. *J. Chem. Phys.* **1993**, *98*, 5648.

(15) Lee, C.; Yang, W.; Parr, R. G. *Phys. Rev. B* **1988**, *37*, 785.

(16) Baker, J.; Muir, M.; Andzelm, J.; Scheiner, A. In *Chemical Applications of Density-Functional Theory*; Laird, B. B., Ross, R. B., Ziegler, T., Eds.; ACS Symposium Series 629; American Chemical Society: Washington, DC, 1996.

(17) Niu, S.; Hall, B. M. *Chem Rev.* **2000**, *100*, 353.

(18) (a) Hay, P. J.; Wadt, W. R. *J. Chem. Phys.* **1985**, *82*, 299. (b) Goddard, W. A., III. *Phys Rev.* **1968**, *174*, 659. (c) Melius, C. F.; Olafson, B. O.; Goddard, W. A., III. *Chem. Phys. Lett.* **1974**, *28*, 457.

(19) (a) Hariharan, P. C.; Pople, J. A. *Chem. Phys. Lett.* **1972**, *16*, 217. (b) Francl, M. M.; Pietro, W. J.; Hehre, W. J.; Binkley, J. S.; Gordon, M. S.; DeFrees, D. J.; Pople, J. A. *J. Chem. Phys.* **1982**, *77*, 3654.

(20) (a) Tannor, D. J.; Marten, B.; Murphy, R.; Friesner, R. A.; Sitkoff, D.; Nicholls, A.; Ringnalda, M.; Goddard, W. A., III.; Honig, B. *J. Am. Chem. Soc.* **1994**, *116*, 11875. (b) Marten, B.; Kim, K.; Cortis, C.; Friesner, R. A.; Murphy, R. B.; Ringnalda, M. N.; Sitkoff, D.; Honig, B. *J. Phys. Chem.* **1996**, *100*, 11775.

(21) (a) Truong, T. N.; Truong, T. T.; Stefanovich, E. V. *J. Chem. Phys.* **1997**, *107*, 1881. (b) Cramer, C. J.; Thrular, D. G. *Chem Rev.* **1999**, *99*, 2161. (c) Oxgaard, J.; Muller, R. P.; Periana, R. A.; Goddard, W. A., III. *J. Am. Chem. Soc.* **2004**, *126*, 352.
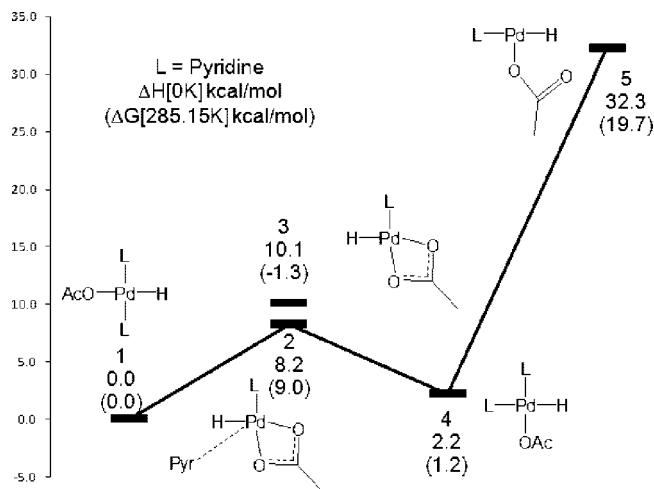
Figure 3. Calculated mechanism for cis/trans isomerization for (pyr)$_2$PdHOAc in toluene.

and no down spin, leading to a total spin projection of $M_S = 1$, commonly referred to as a triplet or spin equal one state, $S = 1$. (Since the up and down spin orbitals need not be equivalent this is referred to as unrestricted DFT, or UDFT.) This state is not strictly an $S = 1$ spin eigenstate (of the spin operator, S^2) since such a Slater determinant wave function can have contributions from higher spins, but this is of little importance for the ground state of O$_2$. A more serious problem occurs for the first excited state of O$_2$, which has $^1\Delta_g$ symmetry with an excitation energy of 22.5 kcal/mol. Here, UDFT (with say up spin for π_{gx} and down spin for π_{gy}) gives an excitation energy of 10.5 kcal/mol, which arises because this $M_s = 0$ wave function has a mixture of $S = 0$ (singlet) and $S = 1$ character. This problem can be treated by applying the spin projection operator, leading to a rigorous singlet excited state and a singlet–triplet splitting of 20.5 kcal/mol.[22a,b] In this case neither the orbitals nor the geometry are optimum after spin projection. Of course one can optimize the orbitals after spin projection as in the GVB method, but this has not been implemented in DFT software. Since the $M_S = 0$ state has nearly equal $S = 0$ and $S = 1$ character, Bally and Borden suggested simply doubling the calculated energy gap, yielding an energy gap of 21.0 kcal/mol for O$_2$.[22c]

All results reported here are UDFT.

3. Results and Discussion

3.1. Cis/Trans Isomerization. As mentioned above we consider that both cis and trans species (**1** and **4**) are important in these catalytic processes as it is likely that both exist in the reaction mixture. In addition to using both cis and trans as starting points for the reoxidation, we also examined the interconversion between the two (Figure 3). The relative stability of structures **2** and **3** ($\Delta H = 8.2$ and 10.1 kcal/mol) differ only by the inclusion of a free pyridine molecule, with **3** being downhill 1.3 kcal/mol on the free energy surface. This stability is due largely to the ability of the OAc ligands to bind η^2 maintaining the square planar Pd^{II} geometry as can be seen by comparing **3** directly with **5** (the result of losing the pyridine cis to the acetate in the trans species) where the acetate cannot bind η^2 and as a result the Pd^{II} T-complex is significantly uphill ($\Delta H = 32.3$ kcal/mol). We did not find rigorous transition states for the conversion between **2** and **1** or **3** but examined constrained pathways for the surrounding potential energy

surface[23] to obtain approximate barriers of 15.1 kcal/mol for **2** → **1** and 13.8 kcal/mol **2** → **4** ($\Delta G^{\ddagger}_{approx} = 16.3$ and 14.9 kcal/mol).

3.2. Direct Insertion Pathway. 3.2.1. Trans Pathway. Starting from *trans*-(pyridine)$_2$-Pd^{II}HOAc (**1**, Figure 4), we introduced (triplet) molecular oxygen which leads immediately to the formation of a weakly bound van der Waals complex [(pyr)$_2$PdHCl]·O$_2$ **6$_{trip}$** with $\Delta H = -0.1$ kcal/mol. There is negligible electron transfer between the O$_2$ and the Pd complex. Spin analysis shows that all unpaired spins in **6$_{trip}$** are on the O$_2$ fragment (one π^* orbital in the plane, hereafter the σ electron, and the other π^* orbital perpendicular to the plane, hereafter the π electron).

From **6$_{trip}$** we find the transition state for direct O$_2$ insertion. Here the transition state, **TS6–7** (Figure 5, left), has the triplet O$_2$ positioned to abstract the H from the Pd with $\Delta H^{\ddagger} = 12.1$ kcal/mol. Thus, from **1** to **TS6–7** the Pd–H bond length stretches from 1.55 to 1.68 Å, indicating a decrease in bond order from 1 to ∼0.7. At the same time the O–O bond distance increases from 1.20 to 1.27 Å, indicating a decrease in bond order of ∼0.2. On the other hand, the O–H distance of 1.30 Å (compared to 0.96 Å in HO$_2$) indicates the O–H bond has not yet formed. At this point the π unpaired spin (perpendicular to the O$_2$–H–Pd plane) remains on the O$_2$, while the σ unpaired spin (in the plane) has partly delocalized onto the Pd d$_{x^2-y^2}$ orbital (where Pd–H is the x direction and the plane is the xy plane). Spin population for the O$_2$ moiety is 1.43 (with 0.66 on the O nearest to Pd), and that for Pd is 0.39.

From **TS6–7** the energy falls monotonically by 17.7 kcal/mol while the HO$_2$ moves out of the square plane toward the OAc ligand to form **7$_{trip}$** in which the H is now bonded to one O of the O$_2$ (H–O = 1.06 Å) while the other O is now directed toward the Pd (Pd–O = 2.48 Å). $\Delta H = -5.6$ kcal/mol with respect to **1**. **7$_{trip}$** is best described as a Pd^I T-complex with unpaired spin in the orbital formerly covalently bonded to the hydride, while the hydrogen in the HO$_2$· radical is coordinating to the *trans*-OAc moiety (H–O$_{\gamma OAc}$ = 1.43 Å). The spin density for the O$_2$ moiety is 1.05 (0.67 of which resides on the O nearest Pd), and that for Pd is 0.78. Since the unpaired orbitals are orthogonal by symmetry and localized on different centers, they have little interaction and **7$_{trip}$** is a biradical. Indeed, the Pd–O bond distance of 2.48 Å indicates little bonding at all, compared to the significantly shorter value of 2.00 Å expected for a Pd^{II}–O single bond. The O–O bond distance of 1.33 Å is typical of a peroxyl radical species (O–O = 1.33 Å in free HO$_2$), halfway between common single- and double-bond distances of 1.48 and 1.21 Å. The O–H bond distance of 0.97 Å is close to that of free HO$_2$· (1.00 Å). Finally, the Pd–O$_{\alpha OAc}$ bond distance of 2.34 Å and the Pd–N distances of 2.15 Å are elongated by 0.26 and 0.06 Å compared to the bond lengths in the corresponding Pd^{II}OOH complex, as expected for a Pd^I center.

Conversion to the singlet state and relaxation leads to **8$_{sing}$**, with $\Delta H = -26.8$ kcal/mol. **8$_{sing}$** is clearly a Pd^{II}OOH complex: the Pd–O bond distance of 2.00 Å is consistent with it being a covalent Pd^{II}–O bond, whereas the O–O bond distance of 1.45 Å is slightly shorter than a normal single-bond distance of 1.48

(22) (a) Xu, X.; Goddard, W. A. *Proc. Natl. Acad. Sci. U.S.A.* **1996**, *99*, 15308. (b) Wittbrodt, J. M.; Schlegel, H. B. *J. Chem. Phys.* **1996**, *105*, 6574. (c) For methods on correcting spin contamination in DFT, see: Bally, T.; Borden, W. T. *Rev. Comput. Chem.* **1999**, *13*, 1.

(23) For both cases the free pyridine in **2** was systematically brought closer to the Pd while being forced to remain 90° from the H for the trans case and 90° from the other pyridine for the cis case.
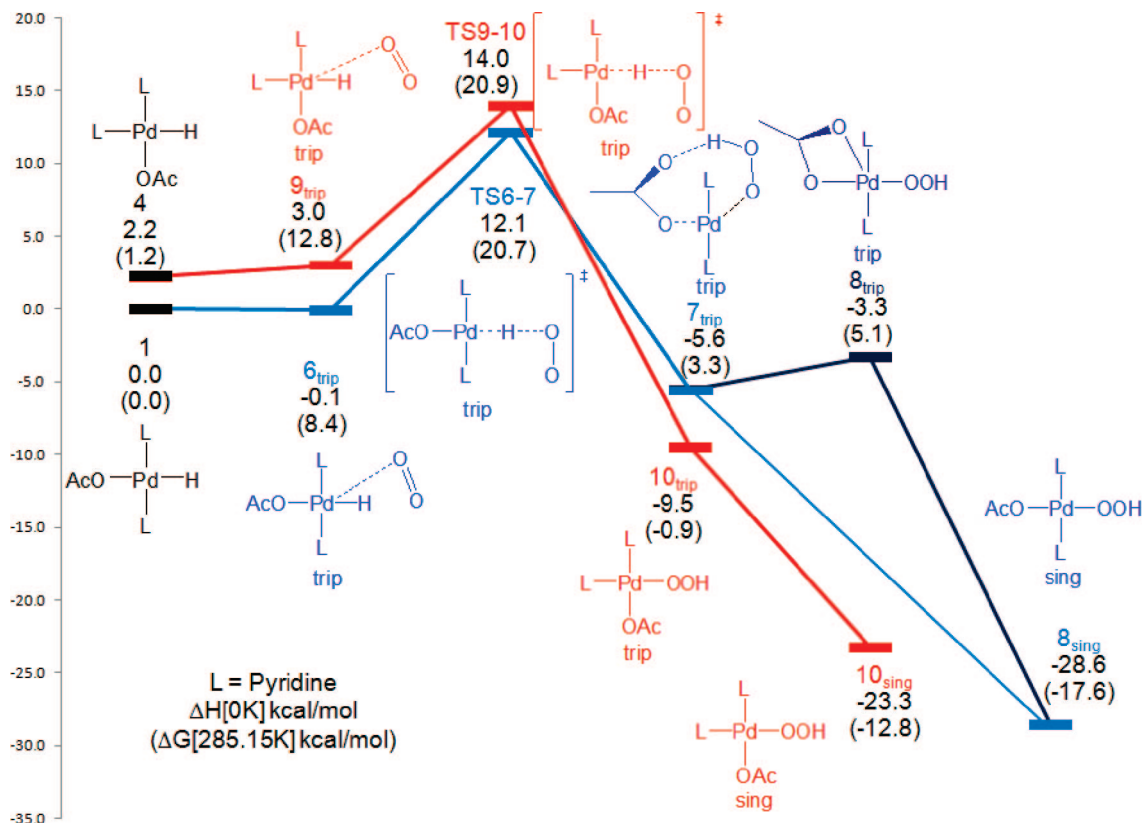
Figure 4. Calculated mechanism for the direct O_2 insertion pathway for $(pyr)_2PdHOAc + O_2 \rightarrow (pyr)_2Pd(OOH)OAc$ in toluene for cis (red line) and trans (blue and navy lines).
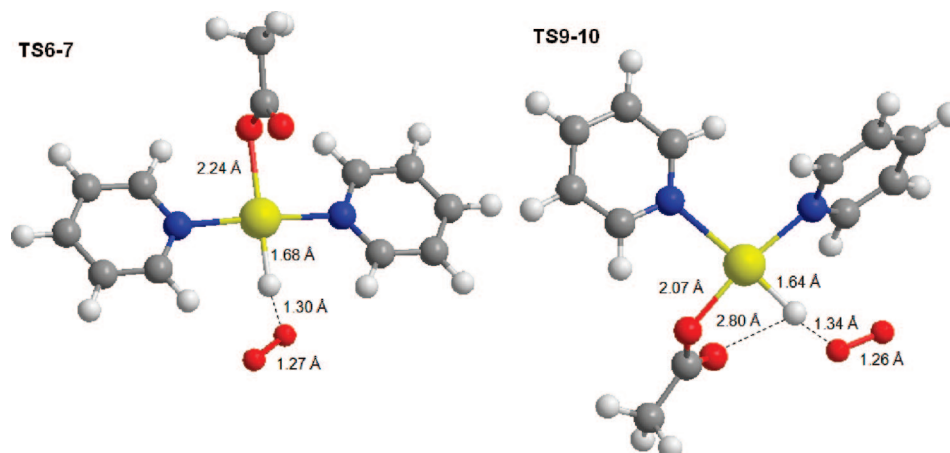

Figure 5. Detailed transition state structures along the trans (left) and cis (right) direct O_2 insertion pathways.

Å. The O−H bond distance of 0.97 Å is consistent with an O−H bond distance in H_2O_2. The Pd−O_{OAc} bond distance of 2.08 Å and the Pd−N distances of 2.09 and 2.10 Å are as expected for Pd^{II}.

As discussed in section 1 spin conversions in related complexes have been thoroughly examined so that it is unnecessary to calculate a MECP for the conversion of 7_{trip} to 8_{sing}. Alternatively rearrangement from 7_{trip} can lead slightly uphill to species 8_{trip}, $\Delta H = -3.3$ kcal/mol as shown in Figure 4. This species is very similar to 7_{trip} except for the loss of H-bonding between the hydroperoxo H and the OAc group, a decrease in Pd−O distance to 2.06 Å, and an increase in the O−Pd−O angle from 120.3° to 168.9°. Conversion to the singlet state and relaxation again leads to 8_{sing}, and we feel it provides no new information to examine the MECP for the conversion

of 8_{trip} to 8_{sing}. From here reaction with a second equivalent of HOAc completes the catalytic cycle by producing $Pd^{II}OAc_2$ and H_2O_2.

3.2.2. Cis Pathway. Starting from *cis*-(pyridine)$_2$-Pd^{II}HOAc (**4**, Figure 4, $\Delta H = 2.2$ kcal/mol) we introduced (triplet) molecular oxygen which leads immediately to the formation of a weakly bound van der Waals complex $[(pyr)_2Pd^{II}HCl] \cdot O_2$ 9_{trip} with $\Delta H = -3.0$ kcal/mol. There is negligible electron transfer between the O_2 and the Pd complex. Spin analysis shows that all unpaired spins in 7_{trip} are on the O_2 fragment (one $\pi*$ orbital in the plane, hereafter the σ electron, and the other $\pi*$ orbital perpendicular to the plane, hereafter the π electron).

From 7_{trip} we find the transition state for direct O_2 insertion. Here the transition state, **TS9−10** (Figure 5, right), has the triplet O_2 positioned to abstract the H from the Pd with $\Delta H^{\ddagger} = 14.0$
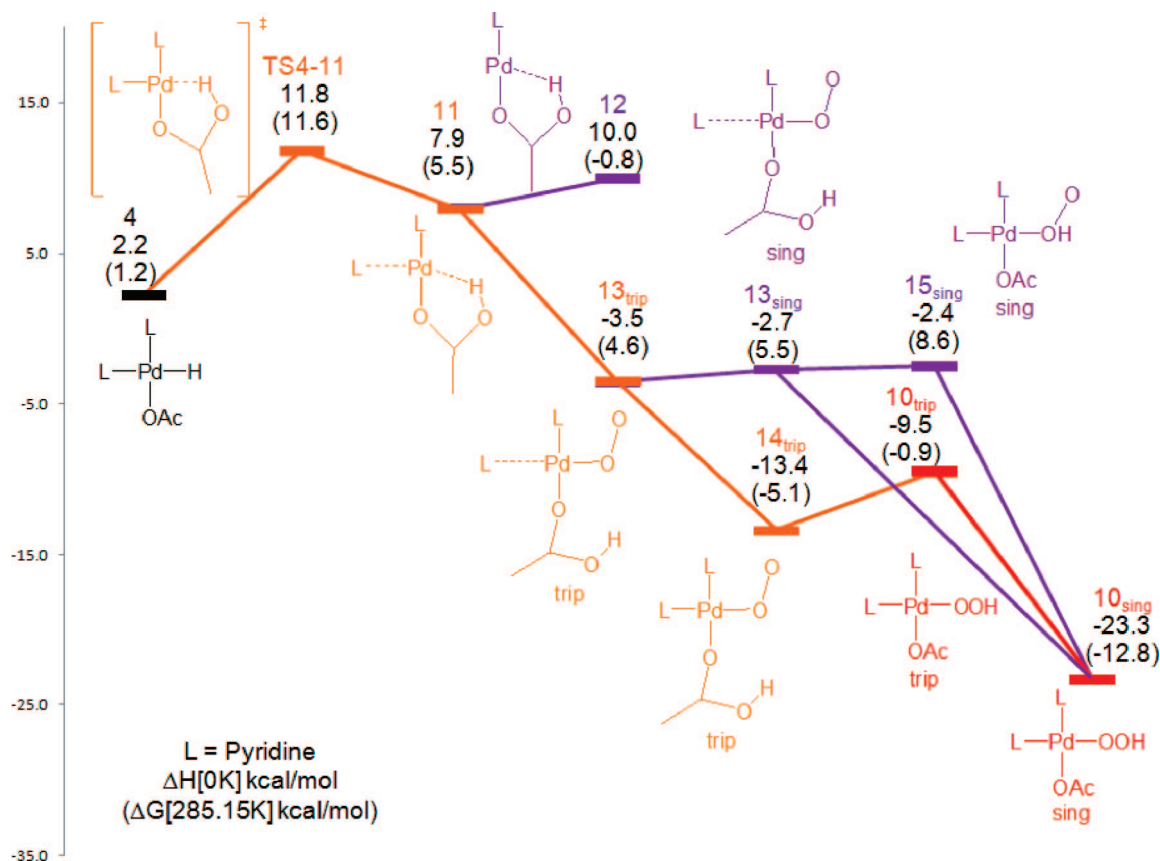
Figure 6. Calculated mechanism for the Pd⁰ pathway for *cis*-(pyr)₂PdHOAc + O₂ → *cis*-(pyr)₂Pd(OOH)OAc in toluene.
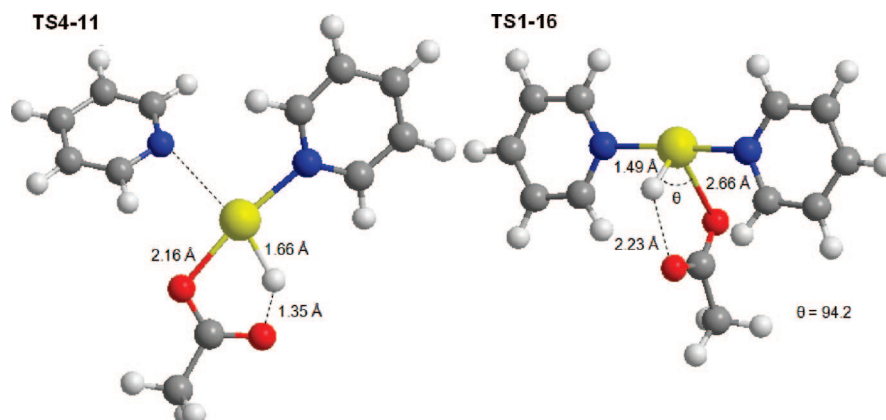

Figure 7. Detailed transition state structures along the cis (left) and trans (right) Pd⁰ pathways.

kcal/mol. Thus, from **4** to **TS9–10** the Pd–H bond length stretches from 1.53 to 1.64 Å, indicating a decrease in bond order from 1 to ∼0.7. Simultaneously, the O–O bond distance increases from 1.20 to 1.26 Å, indicating a decrease in bond order of ∼0.2. On the other hand, the O–H distance of 1.40 Å (compared to 0.96 Å in HO₂) indicates the O–H bond has not yet formed. At this point the π unpaired spin (perpendicular to the O₂–H–Pd plane) remains on the O₂, while the σ unpaired spin (in the plane) has partly delocalized onto the Pd $d_{x^2−y^2}$ orbital (where Pd–H is the x direction and the plane is the xy plane). Spin population for the O₂ moiety is 1.52 (with 0.72 on the O nearest to Pd), and that for Pd is 0.40.

From **TS9–10** the energy falls monotonically by 17.7 kcal/mol while the HO₂ moves out of the square plane toward the OAc ligand to form **10₍trip₎** in which the H is now bonded to one O of the O₂ (H–O = 1.09 Å) while the other O is now bound

to the Pd (Pd–O = 2.26 Å). ΔH = −9.5 kcal/mol with respect to **1**. **10₍trip₎** is best described as a square planar Pd¹ complex with unpaired spin in the orbital formerly covalently bonded to the hydride, while the HO₂• is coordinating to the Pd (H–O₍γOAc₎ = 1.43 Å). The spin density for the O₂ moiety is 1.04 (0.66 of which resides on the O nearest Pd), and that for Pd is 0.78. Since the unpaired orbitals are orthogonal by symmetry and localized on different centers, they have little interaction and **10₍trip₎** is a biradical. Indeed, the Pd–O bond distance of 2.26 Å indicates a weak donor−acceptor bond, compared to the significantly shorter value of 2.00 Å expected for a Pd¹¹−O single bond. The O–O bond distance of 1.33 Å is typical of a peroxyl radical species (O–O = 1.33 Å in free HO₂), halfway between common single- and double-bond distances of 1.48 and 1.21 Å. The O–H bond distance of 1.09 Å is slightly elongated compared to that of free HO₂• (1.00 Å). Finally, the Pd–O₍αOAc₎
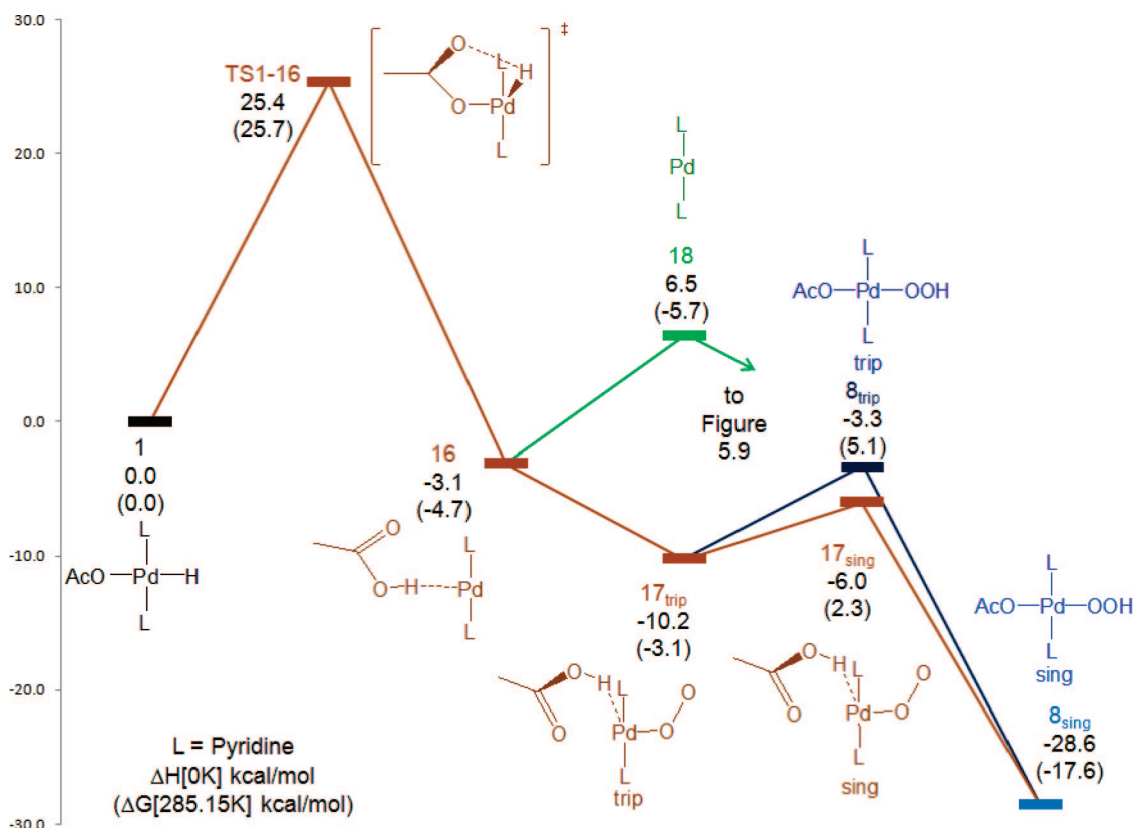
Figure 8. Calculated mechanism for the Pd^0 pathway for *trans*-(pyr)$_2$PdHOAc + O$_2$ → *trans*-(pyr)$_2$Pd(OOH)OAc in toluene (continued from species **13** on Figure 9).

bond distance of 2.27 Å and the Pd−N distances of 2.25 Å for both the cis and trans N's are elongated by 0.20, 0.10, and 0.12 Å compared to the bond lengths in the corresponding Pd^{II}OOH complex, as expected for a Pd^I center.

Conversion to the singlet state and relaxation leads to **10**$_{sing}$, with $\Delta H = -23.3$ kcal/mol. **10**$_{sing}$ is clearly a Pd^{II}OOH complex: the Pd−O bond distance of 1.97 Å is consistent with it being a covalent Pd^{II}−O bond, whereas the O−O bond distance of 1.43 Å is slightly shorter than a normal single-bond distance of 1.48 Å. The O−H bond distance of 0.98 Å is consistent with an O−H bond distance in H$_2$O$_2$. The Pd−O$_{OAc}$ bond distance of 2.07 Å and the Pd−N distances of 2.15 (cis to OAc) and 2.13 Å (trans to OAc) are as expected for Pd^{II}. As discussed earlier, spin conversions in related complexes have been thoroughly examined, and we feel it is unnecessary to calculate a MECP for the conversion of **10**$_{trip}$ to **10**$_{sing}$. From here reaction with a second equivalent of HOAc completes the catalytic cycle by producing Pd^{II}OAc$_2$ and H$_2$O$_2$.

3.3. Pd^0 Pathway: Unassisted Reductive Elimination of HOAc. 3.3.1. Cis Pathway. Similar to section 3.2.2, we start from *cis*-(pyridine)$_2$-Pd^{II}HOAc (**4**, Figure 6). From **4** we found a reductive elimination transition state, **TS4−11** (Figure 7, left), in which the Pd complex goes through an intermolecular proton transfer from the Pd to the OAc resulting in the formation of a linear (pyr)Pd^0−acetic acid complex, **11**. The $\Delta H^\ddagger$ for **TS4−11** is 11.8 kcal/mol. The Pd−H distance has stretched from 1.53 to 1.66 Å, indicating that the Pd−H bond has not completely broken, whereas the O$_{\gamma OAc}$−H distance has decreased from 3.19 to 1.35 Å, indicating that the O$_{\gamma OAc}$−H bond is not fully formed. The imaginary frequency corresponds to a mode in which the proton transfers from the Pd to O$_{\gamma OAc}$ with little other molecular motion except for slight stretching of the Pd−N (cis to OAc) distance. Also of note is that the Pd−N (cis to OAc) distance

has increased from 2.29 to 2.54 Å, indicating a loss of bonding, consistent with the hybridization of the available orbitals on a d^{10} Pd^0 species. As a result of the change in formal oxidation state of the Pd, the Pd−O$_{\alpha OAc}$ distance has increased from 2.04 to 2.16 Å.

From **TS4−11** the reaction proceeds to species **11**, a linear Pd^0 complex very similar to the preceding transition state. Indeed, the only significant changes are the further stretching of the Pd−H distance to 2.19 Å, the reduction of the O$_{\gamma OAc}$−H distance to 1.01 Å, and further stretching of Pd−N (cis to OAc) distance to 4.30 Å indicating a complete loss of bonding to the second pyridine molecule. Species **4** is downhill with $\Delta H = 7.9$ kcal/mol. Complete removal of the free pyridine, **12**, is uphill only 2.1 kcal/mol (downhill on the free energy surface) but will not be pursued as reintroduction of the pyridine must immediately occur after introduction of O$_2$ to the system.

Instead of removing pyridine, we added triplet dioxygen to **11**. We could not isolate any unbound Pd^0−O$_2$ species, as all attempts immediately optimized to a three-coordinate triplet (pyr)Pd^I(η^1-O$_2$)−acetic acid complex, **13**$_{trip}$, with a ΔH of -3.5 kcal/mol. The new Pd−O$_2$ bond and the electron transfer to form Pd^I are the main factors governing the exothermicity of this step. In this species the N from the bound pyridine, the O$_{\alpha OAc}$, and the bonding O of the end-on O$_2$ moiety, and the Pd all reside in the plane. Spin analysis of complex **5**$_{trip}$ shows a spin density of 1.29 on the two oxygens (0.71 on the O α to Pd and 0.58 on the O β to Pd), a spin density of 0.64 on the Pd atom, and the remaining spin density (0.07) distributed over the bound pyridine and HOAc, indicating that this complex should be considered a Pd^I species. The O−O bond of 1.30 Å is typical for a superoxide species (1.33 Å in free O$_2^-$), halfway between common single- and double-bond distances of 1.48 and 1.21 Å, respectively. The Pd−N distance of 3.97 Å (cis to OAc)
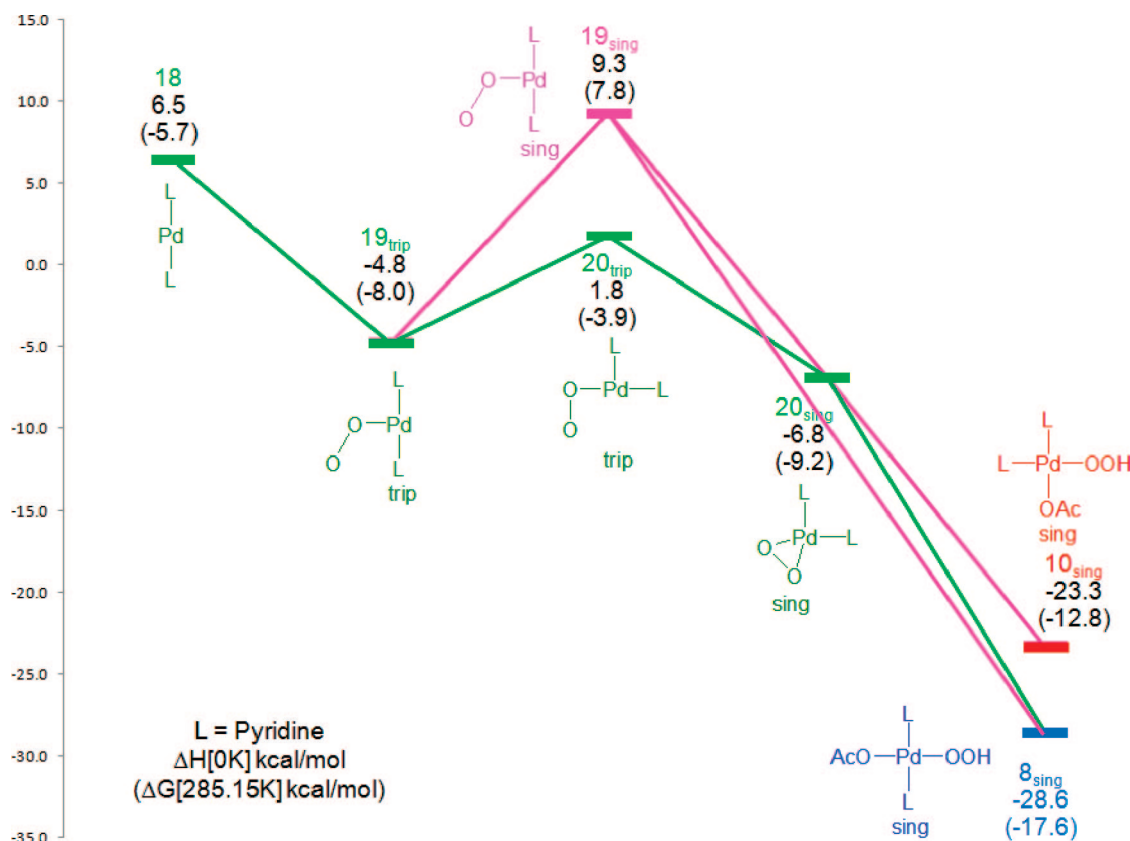
Figure 9. Continuation of the calculated mechanism for the Pd^0 pathway from species **13**.

indicates that the second pyridine remains unbound. The new Pd−O, O−H, and O$_{\gamma OAc}$−H bond lengths are 2.21, 1.55, and 1.12 Å.

At this point coordinating the second pyridine molecule to the Pd center to form species **14**$_{trip}$ is downhill 9.9 kcal/mol (ΔH of −13.4 kcal/mol). The new structure has slightly longer Pd−N bonds of 2.29 Å and a hydrogen bond between the HOAc and the α O of the O$_2$ with a distance of 1.37 Å (down from 1.55 Å in **13**$_{trip}$). From here a proton transfer to the β O of the O$_2$ results in species **10**$_{trip}$ presented above in section 3.2.2 and will not be discussed further. Attempts to transfer the proton to the α O of the O$_2$ while maintaining the triplet spin configuration (**14**$_{trip}$, not shown) were unsuccessful and collapsed to either **10**$_{trip}$ or **14**$_{trip}$.

As an alternate pathway we considered spin conversion from **13**$_{trip}$ before recoordinating the second pyridine molecule to the Pd resulting in species **13**$_{sing}$ (ΔH of −2.7 kcal/mol). From here a proton transfer to the β O of the O$_2$ results in species **10**$_{sing}$ presented above in section 3.2.2 and will not be discussed further. Alternatively proton transfer to the α O of O$_2$ may occur first, **15**$_{sing}$ (ΔH of −2.4 kcal/mol). **15**$_{sing}$ can proceed to species **10**$_{sing}$ through a additional proton transfer to the β O of O$_2$ or could react with a second equivalent of HOAc completing the catalytic cycle by producing Pd^{II}OAc$_2$ and H$_2$O$_2$.

3.3.2. Trans Pathway. Similar to section 3.2.1, we start from *trans*-(pyridine)$_2$-Pd^{II}HOAc (**1**, Figure 8). From **4** we found a reductive elimination transition state, **TS1−16** (Figure 7, right), in which the Pd complex goes through an intermolecular proton transfer from the Pd to the OAc resulting in the formation of a linear (pyr)$_2$Pd^0 complex, **16**. The $\Delta H^{\ddagger}$ for **TS1−16** is 25.4 kcal/mol. This relatively high barrier is thought to be the result of considerable distortion from the square planar starting structure ($\theta = 94.2°$) and the elongation of the Pd−O$_{\alpha OAc}$ distance from

2.18 to 2.66 Å required to gain close proximity between the H and the O$_{\gamma OAc}$. The Pd−H distance has decreased from 1.55 to 1.49 Å, presumably due to the removal of the trans effect from the OAc, whereas the O$_{\gamma OAc}$−H distance has decreased from 3.19 to 2.23 Å, indicating that the O$_{\gamma OAc}$−H bond is not formed. The imaginary frequency corresponds to a mode in which the proton transfers from the Pd to O$_{\gamma OAc}$ with little other molecular motion. Also of note is that the Pd−N distances have had little change increasing from 2.08 to 2.10 Å.[24]

From **TS1−16** the reaction proceeds to species **16**, a linear Pd^0 with acetic acid forming a weakly bound van der Waals complex with the H pointed directly at the Pd. Significant changes in this structure compared to the preceding transient state are the further stretching of the Pd−H distance to 2.14 Å, the reduction of the O$_{\gamma OAc}$−H distance to 1.01 Å, and further stretching of Pd−O$_{\alpha OAc}$ distance to 3.91 Å indicating a complete loss of bonding. Species **16** is downhill with $\Delta H = -3.1$ kcal/mol.

Introduction of triplet oxygen at this point leads directly to a three-coordinate triplet *trans*-(pyr)$_2$Pd$^I(\eta^1$-O$_2$) species with acetic acid still forming a weakly bound van der Waals complex, **17**$_{trip}$. We could not isolate any unbound Pd^0−O$_2$ species, as all attempts immediately optimized to **17**$_{trip}$, with a ΔH of −10.2 kcal/mol. The new Pd−O$_2$ bond and the electron transfer to form Pd^I are the main factors governing the exothermicity of this step. Spin analysis of complex **17**$_{trip}$ shows a spin density of 1.56 on the two oxygens (0.79 on the O α to Pd and 0.77 on the O β to Pd), a spin density of 0.40 on the Pd atom, and the remaining spin density (0.04) distributed over the pyridines and the HOAc, suggesting that this complex should be considered

---

(24) This transition state is almost identical to the corresponding transition state for (IMes)$_2$PdHOAc from ref 8 discussed in section 1.
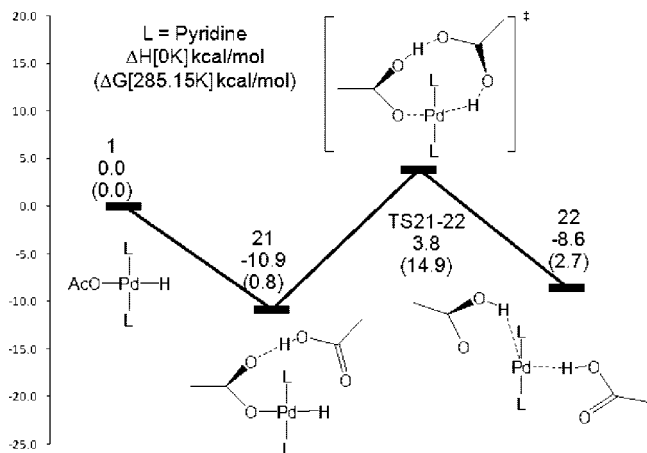
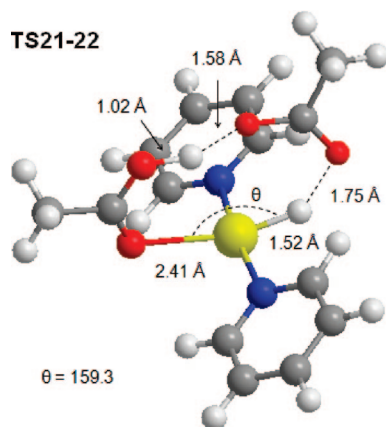**Figure 10.** Calculated mechanism for the Pd⁰ pathway with the inclusion of an additional HOAc molecule.

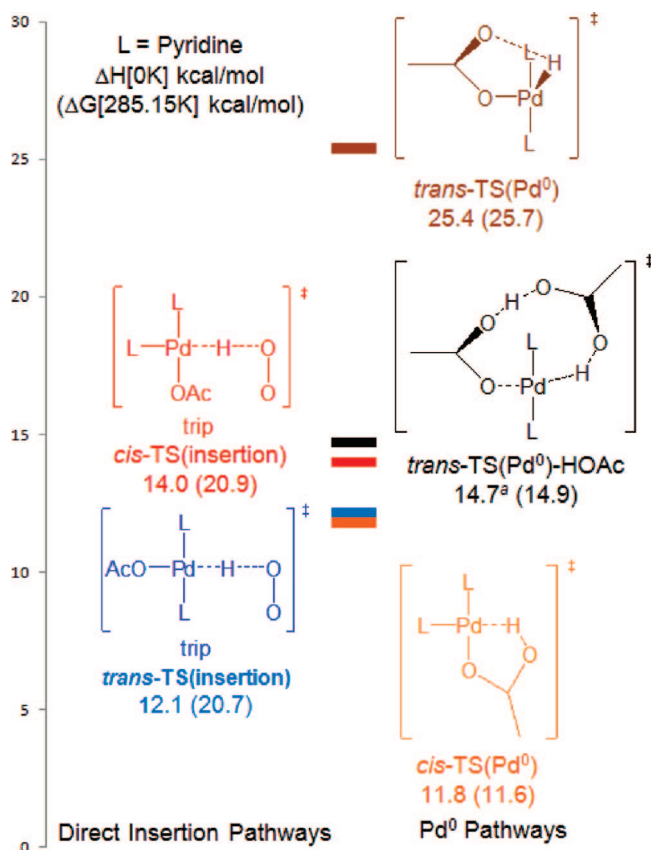**Figure 11.** Detailed transition state structures along the HOAc-assisted Pd⁰ pathways.

Figure 12. Comparison of *cis*-Pd⁰ (orange), *trans*-Pd⁰ (brown), *trans*-Pd⁰ (HOAc-assisted, black), cis-insertion (red), and trans-insertion (blue) transition state energies $(pyr)_2PdHOAc + O_2 \rightarrow (spar)Pd(OOH)OAc$ in toluene. a, ΔH value with respect to *trans*-$(pyr)_2PdHOAc\cdot HOAc$.

a Pd^I species. The O—O bond of 1.27 Å is somewhat shorter than that of superoxide (1.33 Å in free O_2^-), halfway between common single- and double-bond distances of 1.48 and 1.21 Å, respectively. The new Pd—O bond length is 2.34 Å.

At this point spin conversion leads to species 17_{sing} ($\Delta H = -6.0$ kcal/mol) with almost no change in geometry. From here a proton transfer to the β O of the O_2 results in species 8_{sing}, presented above in section 3.2.1 and will not be discussed further. Alternatively the proton transfer to may occur first to form species 8_{trip} followed by the spin conversion once again leading to 8_{sing}.

As an alternative to proceeding through species 17_{trip} we considered complete removal of the HOAc from species **16** leading directly to **18**, which is uphill 9.6 kcal/mol (downhill 1 kcal/mol on the free energy surface). The geometry of **18** is identical to **16** without the HOAc. From **18** addition of O_2 leads directly to a three-coordinate triplet *trans*-$(pyr)_2Pd^I(\eta^1-O_2)$ species (Figure 9). We could not isolate any unbound Pd⁰—O_2 species, as all attempts immediately optimized to 19_{trip}, with a ΔH of -4.8 kcal/mol. The geometry of 19_{trip} is identical to 17_{trip} without the HOAc.

From 19_{trip} it is uphill 6.6 kcal/mol to the corresponding cis species 20_{trip} ($\Delta H = 1.8$ kcal/mol). Spin analysis of complex 17_{trip} shows a spin density of 1.40 on the two oxygens (0.76 on the O α to Pd and 0.64 on the O β to Pd), a spin density of 0.54 on the Pd atom, suggesting that this complex should be considered a Pd^I species. The O—O bond of 1.30 Å is similar to that of superoxide (1.33 Å in free O_2^-), halfway between

common single- and double-bond distances of 1.48 and 1.21 Å, respectively. The new Pd—O bond length is 2.06 Å.

At this point spin conversion leads to species 20_{sing} ($\Delta H = -6.8$ kcal/mol). The new O—O bond distance is slightly longer (1.38 Å) and the new Pd—O bond lengths are 2.00 Å. From here, reaction with HOAc results in either species 8_{sing} (section 3.2.1) or 10_{sing} (section 3.2.2) and will not be discussed further. Alternatively spin conversion could occur at 19_{trip} resulting in 19_{sing} with $\Delta H = 9.3$ kcal/mol. From here rearrangement to 20_{sing} is feasible or direct reaction with HOAc result in either species 8_{sing} or 10_{sing} and will not be discussed further.

3.4. Pd⁰ Pathway: HOAc-Assisted Reductive Elimination of HOAc. Section 3.3.2 demonstrated that direct reductive elimination of HOAc from *trans*-(pyridine)$_2$-Pd^{II}HOAc is considerably high in energy. As an alternative pathway for this process we examined assisted reductive elimination in which an additional HOAc molecule (present in catalytic systems) was added and optimized. From **4** we first found a stable van der Waals complex between *trans*-(pyr)$_2$PdHOAc and the added HOAc (Figure 10, **21**). The additional acid molecule lies out of the plane forming hydrogen bonds to the H of the Pd complex (O—H distance = 1.61 Å). ΔH for this is -10.9 kcal/mol ($\Delta G = 0.8$ and further ΔH's for the HOAc-assisted steps will be with respect to this species referred to as ΔH^a).

Next we found an acid-assisted reductive elimination transition state, **TS21—22** (Figure 11), in which the Pd complex goes through a proton transfer from the Pd to the OAc with the aid of the additional HOAc molecule (now HOAc$_{add}$) resulting in the formation of a linear (pyr)$_2$Pd⁰ complex, **22**. The $\Delta H^‡$ for **TS21—22** is 3.8 kcal/mol ($\Delta H^{‡a} = 14.7$ kcal/mol). This barrier

is considerably lower (both ΔH^a and ΔG) than the unassisted pathway present above. This difference is most likely a result of relaxation toward the square planar starting structure ($\theta = 159.3°$) and the shorter Pd$-$O$_{\alpha OAc}$ distance of 2.41 Å. The transition state is a distorted nine-member ring consisting of Pd with both carboxylic acid moieties. The Pd$-$H distance now decreases only from 1.55 to 1.52 Å, whereas the O$_{\gamma OAc}-$H$_{add}$ distance has decreased from 1.54 to 1.02 Å, indicating that the O$_{\gamma OAc}-$H$_{add}$ bond has already formed. The H$_{add}-$O$_{add}$ distance has increased to 1.58 Å on the order of a H-bond, whereas the O$_{add}-$H$_{Pd}$ distance is now 1.75 Å. The imaginary frequency corresponds primarily to a mode in which H$_{Pd}$ transfers from the Pd to O$_{add}$ with H$-$O$_{\gamma OAc}$ and Pd$-$O$_{\alpha OAc}$ stretching to a lesser extent. Despite the almost complete transfer of H$_{add}$ in this transition state, it is the concerted dual proton transfer transition state and not simply a proton transfer from Pd-(HOAc)H$^+$ to OAc$^-$, as examination of the intermediates directly preceding and following this transition state are indeed **21** and **22**. From **22** this pathway can join the previously presented mechanism at species **16** in Figure 8.

4. Conclusions

We conclude that the Pd^0 reductive elimination pathway and the direct insertion pathway as presented above are both feasible for (pyr)$_2$PdXOAc. In addition we outlined five competing pathways involving the cis and trans forms of the hydride as well as the incorporation of an additional HOAc molecule. The five different pathways proceed as follows:

1. *trans*-(Pyr)$_2$PdOAcH direct insertion involves first the abstraction of the H atom from the palladium center ($\Delta H^‡ = 12.1$ kcal/mol, $\Delta G^‡ = 20.7$ kcal/mol, Figure 12, blue) and the immediate formation of *trans*-(pyr)$_2$Pd^{I}OAc/HOO• triplet van der Waals complex. This then undergoes spin conversion to singlet and relaxation to form *trans*-(pyr)$_2$Pd(OOH)OAc. Reaction with a second equivalent of HOAc completes the catalytic cycle by producing Pd^{II}OAc$_2$ and H$_2$O$_2$.

2. *cis*-(Pyr)$_2$PdOAcH direct insertion involves first the abstraction of the H atom from the palladium center ($\Delta H^‡ = 14.0$ kcal/mol, $\Delta G^‡ = 20.9$ kcal/mol, Figure 12, red) and the immediate formation of *cis*-(pyr)$_2$Pd^I(OOH)OAc triplet. This then undergoes spin conversion to the *cis*-(pyr)$_2$Pd-(OOH)OAc singlet. Reaction with a second equivalent of HOAc completes the catalytic cycle by producing Pd^{II}OAc$_2$ and H$_2$O$_2$.

3. *cis*-(Pyr)$_2$PdOAcH Pd^0 reductive elimination pathway involves first the intramolecular migration of the hydride to form HOAc while maintaining the interaction between the OAc moiety and the Pd ($\Delta H^‡ = 11.8$ kcal/mol, $\Delta G^‡ = 11.6$ kcal/mol, Figure 12, orange) and the loss of one of the pyridine ligands (initially trans to H) to form *trans*-(pyr)Pd^0(HOAc). Introduction of O$_2$ and reattachment of the second pyridine results in the formation of *cis*-(pyr)$_2$Pd^I(η^1-O$_2$)(HOAc) triplet which then undergoes a proton transfer followed by spin conversion to the *cis*-(pyr)$_2$Pd(OOH)OAc singlet. Reaction with a second equivalent of HOAc completes the catalytic cycle by producing Pd^{II}OAc$_2$ and H$_2$O$_2$.

4. Unassisted *trans*-(pyr)$_2$PdOAcH Pd^0 pathway involves first the reductive elimination of HOAc from a strained seesaw structure ($\Delta H^‡ = 25.4$ kcal/mol, $\Delta G^‡ = 25.7$ kcal/mol, Figure 12, brown) to form the corresponding *trans*-(pyr)$_2$Pd^0/(HOAc) van der Waals complex. Upon introduc-

tion of O$_2$ and reaction with the HOAc fragment and spin conversion, the reaction proceeds to the *trans*-(pyr)$_2$Pd-(OOH)OAc singlet. Reaction with a second equivalent of HOAc completes the catalytic cycle by producing Pd^{II}OAc$_2$ and H$_2$O$_2$.

5. HOAc-assisted *trans*-(pyr)$_2$PdOAcH Pd^0 pathway involves first the reductive elimination of HOAc from a nearly planar (H$-$Pd$-$O angle $= 159.3°$) through a nine-membered ring transition state with the assistance of a second HOAc molecule ($\Delta H^{‡a} = 14.7$ kcal/mol, $\Delta G^‡ = 14.9$ kcal/mol, Figure 12, black) to form the corresponding *trans*-(pyr)$_2$Pd^0/(HOAc) van der Waals complex. Upon introduction of O$_2$, reaction with the HOAc fragment and spin conversion the reaction proceeds to the *trans*-(pyr)$_2$Pd(OOH)OAc singlet. Reaction with a second equivalent of HOAc completes the catalytic cycle by producing Pd^{II}OAc$_2$ and H$_2$O$_2$.

The barrier for the *cis*-Pd^0 pathway is lower than that of the direct oxygen insertion mechanism ($\Delta\Delta H^‡ = 2.2$ kcal/mol, $\Delta\Delta G^‡ = 9.3$ kcal/mol), and the barrier for the HOAc-assisted *trans*-Pd^0 pathway is lower than that of the direct oxygen insertion mechanism ($\Delta\Delta H^‡ = -2.6$ kcal/mol, $\Delta\Delta G^‡ = 5.8$ kcal/mol). In addition the barrier for *cis*-Pd^0 pathway is the lowest overall with ($\Delta H^‡ = 11.8$ kcal/mol, $\Delta G^‡ = 11.6$ kcal/mol). We also calculated a barrier for the cis/trans isomerization ($\Delta H^‡ = 15.1$ kcal/mol, $\Delta\Delta G^‡ = 16.3$ kcal/mol) leading to the conclusion that interconversion does not occur before interaction with oxygen for either the cis or trans cases. However, we still stress the concern that both the cis and trans species are likely to be present in catalytic systems. We expect these results should apply to similar Pd systems that employ two monodentate donor ligands and a basic chelating X-ligand and that our *cis*-Pd^0 pathway and HOAc-assisted-Pd^0 might resolve some of the issues experienced in calculations of other ligand frameworks.

These results demonstrate that incorporation of two monodentate ligands significantly favors the Pd^0 pathways by allowing the formation of a linear Pd^0 complex. This preference for the Pd^0 path differs from that seen with our previous work on bidentate ligand systems. In addition, the chelating OAc moiety avoids the need of an exogenous base.

This work, considered together with our previous reports,[7] now presents a complete picture of the two competing pathways at work in palladium oxidase systems with both a single bidentate ligand or two monodentate ligands (both cis and trans) coupled with multiple X-ligands (OAc and Cl) in the presence of both exogenous acid or base consistent with reaction conditions. This provides a thorough framework for reactions of molecular oxygen with palladium hydrides.

Supporting Information Available: Tables of geometries, ZPE and solvent corrections, and absolute energies of intermediates, as well as geometries, ZPE and solvent corrections, absolute energies, and imaginary frequencies of transition states. This material is available free of charge via the Internet at http://pubs.acs.org.